Non-Destructive Integration of Spark-Discharge Produced Gold Nanoparticles onto Laser-Scribed Graphene Electrodes for Advanced Electrochemical Sensing Applications

Saptami Suresh Shetty , Lavita Nuraviana Rizalputri , Maria G. Trachioti , Saravanan Yuvaraja , Veerappan Mani , Mamas I. Prodromidis , Khaled Nabil Salama

PII: S2468-0230(24)01518-9
DOI: https://doi.org/10.1016/j.surfin.2024.105362
Reference: SURFIN 105362

To appear in: *Surfaces and Interfaces*

Received date: 26 April 2024
Revised date: 10 October 2024
Accepted date: 27 October 2024

Please cite this article as: Saptami Suresh Shetty , Lavita Nuraviana Rizalputri , Maria G. Trachioti , Saravanan Yuvaraja , Veerappan Mani , Mamas I. Prodromidis , Khaled Nabil Salama , Non-Destructive Integration of Spark-Discharge Produced Gold Nanoparticles onto Laser-Scribed Graphene Electrodes for Advanced Electrochemical Sensing Applications, *Surfaces and Interfaces* (2024), doi: https://doi.org/10.1016/j.surfin.2024.105362

Non-Destructive Integration of Spark-Discharge Produced Gold Nanoparticles onto Laser-Scribed Graphene Electrodes for Advanced Electrochemical Sensing Applications

Saptami Suresh Shetty,[1] † Lavita Nuraviana Rizalputri,[1]† Maria G. Trachioti,[2] Saravanan Yuvaraja[1], Veerappan Mani,*[1] Mamas I. Prodromidis,*[2] Khaled Nabil Salama*[1]

[1]Sensors Lab, Advanced Membranes and Porous Materials Center, Computer, Electrical and Mathematical Science and Engineering Division, King Abdullah University of Science and Technology (KAUST), Saudi Arabia.
[2]Department of Chemistry, *University of Ioannina*, 45 110, Ioannina, Greece.

† Authors contributed equally.

Abstract

Gold nanoparticles (AuNPs) decorated graphene materials are preferable materials in a wide range of electrochemical applications, however, the current methods for preparing them have several limitations. Herein, we have developed a green, solution-free, and non-destructive method for the in-situ generation of AuNPs on laser-scribed graphene electrodes (LSGEs), addressing the limitations of traditional preparation methods. This novel technique, contrasting with the conventional solution-based electrochemical deposition, utilizes spark discharge to modify LSGEs, demonstrating superior performance in sensors and biosensors applications. Through comprehensive characterizations (scanning electron microscopy (SEM), energy-dispersive X-ray spectroscopy (EDS), Raman spectra, X-ray diffraction (XRD), X-ray photoelectron spectroscopy (XPS), and Kelvin probe force microscopy (KPFM)), we observed significant distinctions in particle size, metal loading, stability, surface-to-volume ratio, and graphene quality between spark-discharge produced AuNPs (SP-AuNPs) and electrodeposition produced AuNPs (EC-AuNPs). The average particle sizes of the SP-AuNPs and EC-AuNPs are 10 nm and 38 nm, respectively. The SP-AuNPs modified LSGEs demonstrate exceptional electroanalytical performance in dopamine detection, with a broad detection range (0.6–90 µM) and low LOD (0.40 µM), further validated in human neuroblastoma cells SH-SY5Y. Our findings suggest that the spark discharge method represents a significant advancement in the synthesis of metal nanoparticle enhanced LSG electrodes, with broad implications for electrochemical sensing, biosensing, and biomedical applications.

Keywords: Laser-scribed graphene; Metal nanoparticles; Spark discharge; Electrochemical sensors; Biosensors; Electroanalysis.

1. Introduction

Laser-scribed graphene electrodes (LSGE) have emerged as a new generation of electrodes in electrochemical applications, finding diverse applications from clinical diagnostics to environmental monitoring [1-3]. LSGE fabrication stands out for its direct, mask-free patterning through laser irradiation, yielding electrodes with high electrical conductivity, mechanical stability, enhanced ionic mobility, and highly porous graphene structures [4-6]. Functionalization of LSGEs with metal nanoparticles, including gold, silver, and platinum, by doping during laser writing, significantly boosts their electrochemical activity, surface area, and biosensing capabilities [7-10].

Gold nanoparticles (AuNPs) are particularly valued for their unique physicochemical properties, such as optical characteristics, biocompatibility, catalytic efficiency, conductivity, and high surface-to-volume ratio, making them ideal for enhancing LSGE performance [11-13]. Mounting evidences demonstrated the exceptions performance of AuNPs-modified LSGEs in detecting various biomarkers including acetaminophen [14], glucose [15], hydrogen peroxide [16], and bisphenol A [17], alongside their use in constructing advanced biosensors including aptasensors [18], immunosensors [19], molecularly imprinting polymer-based electrodes [20]. Noteworthy examples include the development of a smartphone-based aptasensor for cardiac troponin I quantification [21], an interdigitated immunosensor array for *Escherichia coli O157:H7* detection [8] and point-of-care aptasensor for human epidermal growth factor receptor 2 (HER-2), showcasing the broad potential of AuNP/LSGE in point-of-care diagnostics and beyond [22].

However, the predominant electrochemical synthesis of AuNPs through electrodeposition faces significant challenges, such as the necessity for extensive washing, poor film stability, and the potential for graphene damage due to acidic conditions [20]. Especially, electrodeposition is a solution-based process that bring inherent limitations such as waste generation and nanoparticle aggregation [23]. An alternative method that is green, solution-free, and non-destructive is therefore urgently required to advance LSGE-AuNP-based electrochemical sensors and biosensors. These limitations highlight the urgent need for an alternative, more sustainable synthesis approach for AuNP/LSGE.

In this direction, the spark-discharge is emerging as a versatile technique for preparing metal nanoparticles [24-27]. The experimental setup is straightforward, consisting of a high voltage (HV) power supply, two electrodes connected as anode and cathode separated by air or a gas flow (i.e., the dielectric medium), and a capacitor connected in parallel with the power supply terminals. The HV power supply delivers current that charges the capacitor until the voltage between the electrodes reaches the breakdown voltage of the dielectric medium. Subsequently, a spark discharge occurs, and the process repeats itself with a frequency determined by the capacitance of the capacitor. The spark discharge induces a current flow, leading to the formation of a conductive plasma channel containing electrons and ionized gas

species. Accompanying the spark discharge, high temperatures (> 20000 K) develop at the sparking point, causing the evaporation of material from both electrodes in the vicinity of the sparking point. This evaporation results in the formation of a vaporized cloud containing species from both electrodes, and after a rapid cooling process, solidification occurs in the form of nano-sized deposits on the electrode surface. A detailed description of the sparking process can be found in the literature [28, 29].

The primary objective of this work is to develop a solution-free, solid-state synthesis method for AuNP/LSGE using the spark-discharge technique. By leveraging a eutectic gold-silicon alloy (eAu/Si) electrode tip on LSGE surfaces, we aim to enhance the surface properties, chemical composition, and electrochemical performance of LSGEs beyond what is achievable with conventional methods. The key advantages of the spark-discharge method are (1) simple synthesis – it only requires a power supply and a metal pin, (2) Green synthesis – no use of acid solutions or other chemicals, (3) extremely fast – less than two minutes required to prepare 10 electrodes and (4) template-free – enables the generation of nanoparticles with high surface purity [30]. As a proof-of-concept, we focus on the electroanalysis of dopamine, a critical neurotransmitter in the diagnosis and understanding of neurological disorders on [31]. The performance of spark discharge produced AuNPs (SP-AuNP) and electrochemically prepared AuNPs (EC-AuNPs) are evaluated and compared. The SP-AuNP/LSGE sensor's ability to detect dopamine with high sensitivity in biological systems represents a significant step forward in the development of diagnostic tools, drug delivery systems, and personalized medicine for neurodegenerative diseases medicine [32].

2. EXPERIMENTAL

2.1. Materials and methods

Potassium ferricyanide ($K_3[Fe(CN)_6]$), Potassium ferrocyanide ($K_4Fe(CN)_6]$) and potassium chloride (KCl) were purchased from MP Biomedicals. Phosphate-buffered saline (PBS) tablets that included 0.0027 M KCl and 0.137 M sodium chloride (NaCl) were purchased from Fisher BioReagents. Commercial polyimide (PI) sheets were purchased from Utech Products, USA, which has a Kapton Width of 12”. Gold (III) chloride hydrate ($HAuCl_4 \cdot xH_2O$), dopamine hydrochloride, ascorbic acid (AA), uric acid (UA), glucose, and human serum sample were obtained from Sigma. All aqueous solution studies employed ultrapure water from a Milli-Q® integrated water purification system (Merck KGaA, Darmstadt, Germany; resistivity: 18.2 MOhm.cm at 25°C). All the compounds were of analytical quality and were utilized as received. Dopamine stock solutions were freshly prepared daily.

Kapton PI film of 12-inch width was purchased from Utech Products, USA, and used as the substrate. A monochromatic Al K X-ray source ($h\nu$=1486.6 eV) operating at 75 W in a vacuum of 1×10^{-8} mbar, a multichannel plate, and a delay line detector were used in the Kratos Axis Supra DLD

spectrometer for the X-ray photoelectron spectroscopy (XPS) studies. The software used for the deconvolution of XPS spectra is CasaXPS. For all element fittings, the Shirley background type was employed to ensure accurate baseline correction. Specifically, the line shapes for different elements were tailored to optimize fitting accuracy. For Au 4f, a combination of asymmetry (A (0.35, 0.5,0)) and Gaussian-Lorentz GL (70) was used. For C1s, the SGL (30,70) line shape was applied; for O1s, SGL (40); and for N1s, SGL (10) was used, providing an optimal fit [33]. X-ray diffraction (XRD) data in the 5–80° range were recorded using an X-ray diffractometer (Bruker Corporation, D8 ADVANCE, and Karlsruhe, Germany). Scanning electron microscopy (SEM) images and Energy-dispersive X-ray spectroscopy (EDS) were carried out using field emission scanning electron microscopy (FESEM, Helios G-5). Raman spectra were obtained with a LabRAM ARAMIS Raman spectrometer (Horiba Scientific) equipped with a 473 nm cobalt laser source at room temperature. The electrochemical measurements were carried out using PalmSens4 (PS41904024817) and MUX8-R2 Multiplexer (MUX8R21904005703) linked to a computer and controlled via PSTrace 5.5 software.

2.2. Fabrication laser-scribed graphene electrodes

A CO_2 Universal Laser Systems® PLS6.75, featuring a 150 μm laser spot diameter and ~10.6 μm wavelength, was utilized for the fabrication of LSGEs. Graphene production occurs via a photothermal process, inducing molecular rearrangements and subsequent formation of graphenic structure. Laser parameters and scribing processes were optimized to ensure high-quality graphene. LSGEs were created on a polyimide sheet using a CO_2 laser under a nitrogen atmosphere, adhering to optimal conditions for quality graphene production. Electrode design and patterning were accomplished using CorelDRAW software, employing a mask-free approach for efficient and precise electrode configuration. Laser parameters such as power, speed, and z distance were fine-tuned for graphene production. The optimization process included adjusting laser scribing speed and power for electrode fabrication and utilizing an inert gas flow to minimize heteroatom bonding. The resistance per square for each laser parameter was carefully checked, resulting in the production of high-quality graphene with 2.8 W power, 2.5 cm/s speed, 1000 pulses per inch, and a 1 mm Z distance, yielding a sheet resistance of 58 Ω/square. Three electrodes (working, reference, and counter) were designed and patterned with dimensions of 2.6 cm × 0.6 cm. The sensing area of the LSG sensor is isolated by a passivation layer between the electrodes and the connection areas.

2.3. Fabrication of spark-discharge AuNP/LSGE and electrochemical AuNP/LSGE

The fabrication methods for both SP-AuNP/LSGE and EC-AuNP/LSGE are illustrated **in Figure 1**. Spark-discharge AuNPs were generated by following our previously reported procedure with

modifications based on optimizations results [27, 30]. Spark modification of the LSGE was performed by connecting the eAu/Si tip electrode and LSGE to an HV power supply. These two materials were brought into proximity using a G-code controlled 3D positioning device until the spark discharge event occurred at 1.2 kV DC at ambient conditions. The LSGE was connected to the positive pole (as an anode) and the eAu/Si tip to the negative pole (as cathode) of the power supply.

Electrodeposited AuNPs were prepared by placing 75 µL of 50 mM $HAuCl_4$ in 0.5 M H_2SO_4 on plain LSGE and by applying a constant potential of −0.90 V for 60 s [34]. The modified LSGEs, i.e., EC-AuNP/LSGEs were washed with DI water and dried with nitrogen gas. The electrodes are stored in a dry box.

2.4. Electrochemical measurements

The electrochemical cell consists of a three-electrode chip, with laser-graphene serving as the reference and counter electrodes, and SP-AuNP/LSGE or EC-AuNP/LSGE serving as the working electrode. All electrochemical studies were carried out at room temperature. The geometrical area of the working electrode was 0.071 cm^2. The chips were connected to an electrochemical workstation using an electrode connector provided by PalmSens. The cell volume was maintained to be 75 µL. The supporting electrolytes was 0.10 M PBS, pH 7.0 for cyclic voltammetry (CV), differential pulse voltammetry (DPV), and electrochemical impedance spectroscopy (EIS) experiments. CV scans (CVs) were recorded within the potential range from − 0.50 to + 0.50 V at a scan rate of 50 mV/s. The DPV scans were recorded over the potential range from – 0.20 V to + 0.40 V by applying the following potential waveform: modulation amplitude, 50 mV/s; step potential, 0.01 V; and t pulse, 20 ms. EIS experiments were conducted in 0.10 M PBS, pH 7 containing 5+5 mM $K_3[Fe(CN)_6]/K_4[Fe(CN)_6]$ at the frequency range of 0.1-100,000 Hz and amplitude 10 mV.

2.5. SH-SY5Y cell culture

The SH-SY5Y cells were cultured in a 60 x 15 mm Petri dish at 37°C and 5% CO_2 with 1.0×10^7 cells/mL density. The medium consisted of 5% Dulbecco's Modified Eagle Medium (DMEM), 1% penicillin-streptomycin, and 10% fetal bovine serum. The cells grown on the Petri dish were recovered using trypsin solution. The number of cells was approximately 1×10^6 cells/cm^2 in the final solution. Automated cell counter (Countess™ 3 FL) was used for counting cells. Next, the solution containing cells were directly transferred to the electrochemical cell. The K^+ stimulation was used to depolarize the live cells and to induce the release of dopamine by exocytosis. Different concentrations of KCl (50 and 100 mM) were co-incubated with the cells, and the *in-situ* production of dopamine was subsequently monitored.

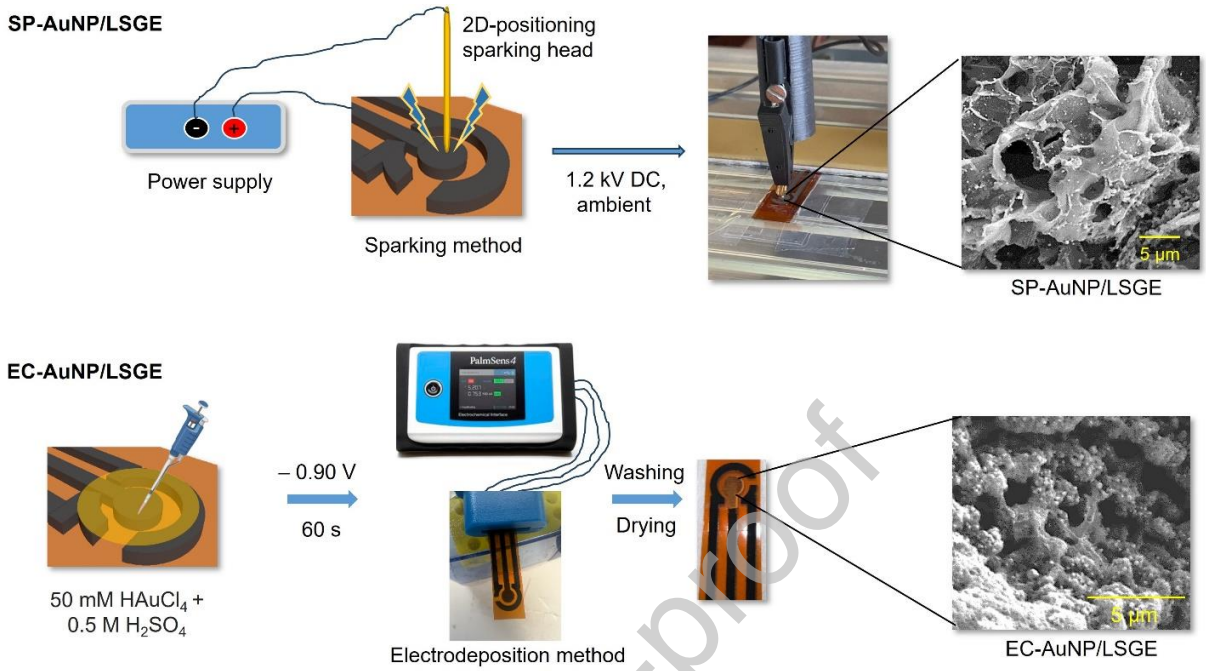

Figure 1. Fabrication procedure for SP-AuNP/LSGE and EC-AuNP/LSGE

3. RESULTS AND DISCUSSIONS

3.1. Physiochemical properties

SEM images of the plain LSGE (**Figure 2**A-C), EC-AuNP/LSGE (**Figure 2**D-F) and SP-AuNP/LSGE (**Figure 2**G-I) are captured at three different magnifications. The plain LSGE displays a typical porous sheet-like morphology, which matches well with the previously reported morphology for LSG electrodes [34]. Both EC-AuNP/LSGE and SP-AuNP/LSGE display a typical morphology of graphene-Au nanocomposites, in which, nanometer-sized particles are adhered on the layered sheets of graphene [35]. The SEM investigation suggests both spark-discharge and electrodeposition methods are successful in producing AuNPs on laser-induced graphene sheets, however, the morphology of the graphene sheets, and size and distribution of AuNPs differ among them. Firstly, the graphene sheet structures are damaged when we analyze the high-resolution image of EC-AuNP/LSGE. However, the graphene structures are perceived in the high-resolution image of SP-AuNP/LSGE, which closely resembles the morphology of unmodified LSGE. This means that the layered sheet-like structure of graphene is not affected by the sparking method, however, it is adversely affected by the electrodeposition method.

To investigate the effect of the electrodeposition process on graphene sheets, the images of the unmodified LSGE that was electrochemically treated with HCl at different deposition times (5 s, 30 s and 60 s) were analyzed (**Figure S1**A-C). Note that, this experiment doesn't contain the precursors of AuNPs. When analyzing the corresponding SEM images, it is found that the LSGE sheets are damaged for all the tested deposition times. The damage is severe when deposition time is increased from 5 s to 60 s. This study confirms that the production of AuNPs through electrochemical method damages the graphene sheets. It is worth mentioning that the large portion of the interesting properties of graphene are originated from its layered structure. Perceiving the layered structure is very important to harvest the full benefits of graphene properties. Interestingly, the preparation process of SP-AuNPs does not involve the use of acidic solutions and hence graphenic structure is perceived even after AuNPs are deposited on LSGEs. Secondly, the average particle size of the AuNPs is relatively small in SP-AuNPs compared with EC-AuNPs. The average particle sizes of the SP-AuNPs and EC-AuNPs are 10 nm and 38 nm, respectively. One potential explanation for this observation is the distinction in the nucleation process between the spark-discharge method and the electrodeposition method. In the electrochemical deposition method, the Au precursor remains continuously connected to the electrode surface, facilitating the rapid reduction of surface energy and the formation of stable, larger particles. In contrast, the sparking method operates in the solid-state, preventing the formation of such larger particles. The rapid cooling of vaporized material in the spark-discharge process may result in unique nucleation characteristics compared with the more controlled and gradual deposition in electrodeposition. The SEM images of EC-AuNPs prepared at different deposition times were also analyzed to see whether the deposition time plays a role in particle size and distribution density. The SEM images of EC-AuNPs prepared at different deposition time intervals are given in **Figure S2**. The particle size of the AuNPs is same for all the examined deposition times, only the density of the particles is increased. This result suggests that the deposition time has no influence on the particle size.

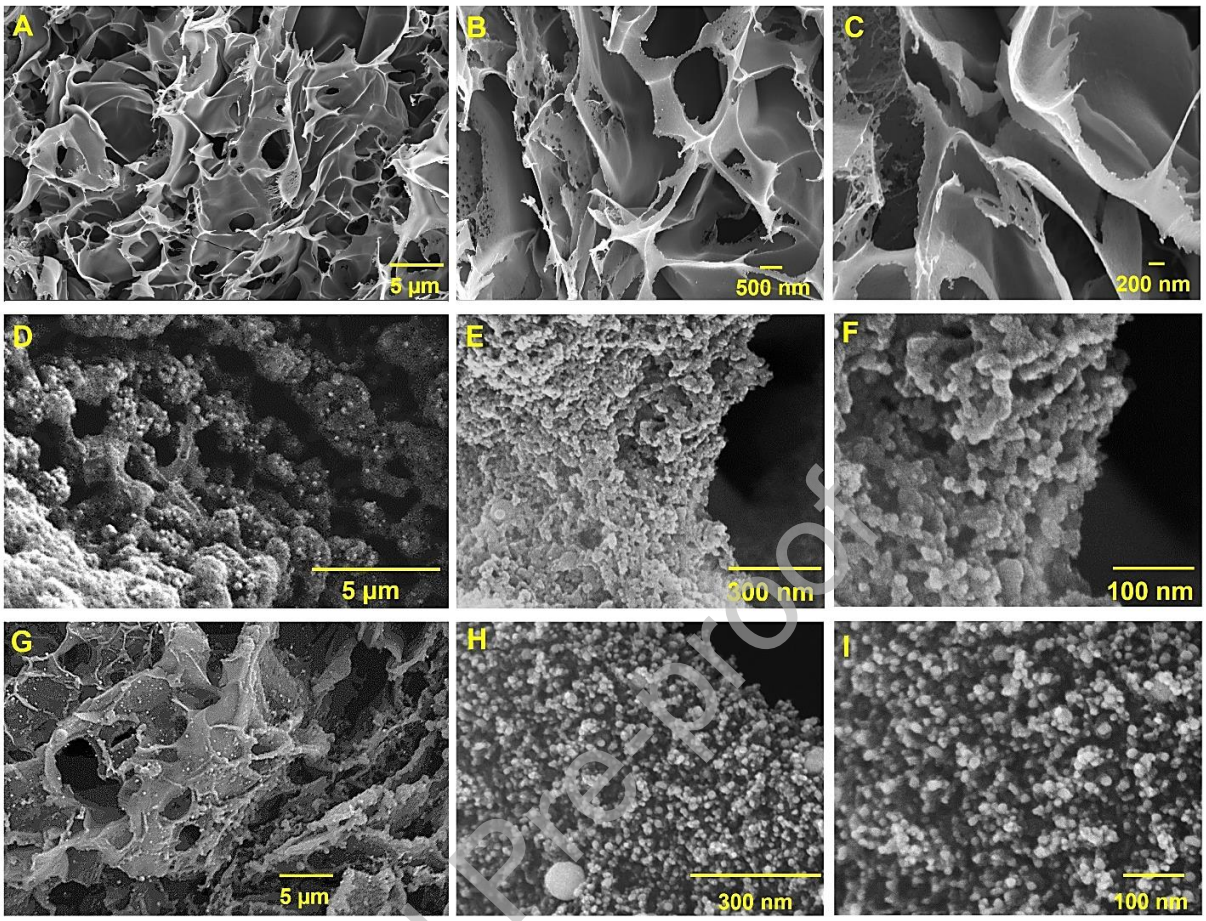

Figure 2. SEM images of plain LSGE (A-C), EC-AuNP/LSGE (D-F), and SP-AuNP/LSGE (G-I).

The EDS spectra of SP-AuNPs, EC-AuNPs, and plain LSGE are shown in **Figure S3**A-C. The presence of Si (~ 3%) is attributed to the eutectic gold silicon alloy (eAu/Si) electrode tip which was used in the sparking process. The atomic percentages of carbon and oxygen at the plain LSGE are 83.12 and 10.70%, respectively. The oxygen signal originates from the oxygen functionalities attached to the graphene sheets [36]. The atomic percentage of carbon, oxygen, and gold atoms at EC-AuNP/LSGE and SP-AuNP/LSGE are 79.91, 2.58, and 10.13%, and 74.75, 2.20, and 9.67%, respectively. As indicated by the EDX data, the atomic percentage of Au is approximately 10% for both EC-AuNPs and SP-AuNPs. To ensure a valid comparison, the Au content in the two electrodes, SP-AuNPs/LSGE and EC-AuNPs, was maintained at the same level.

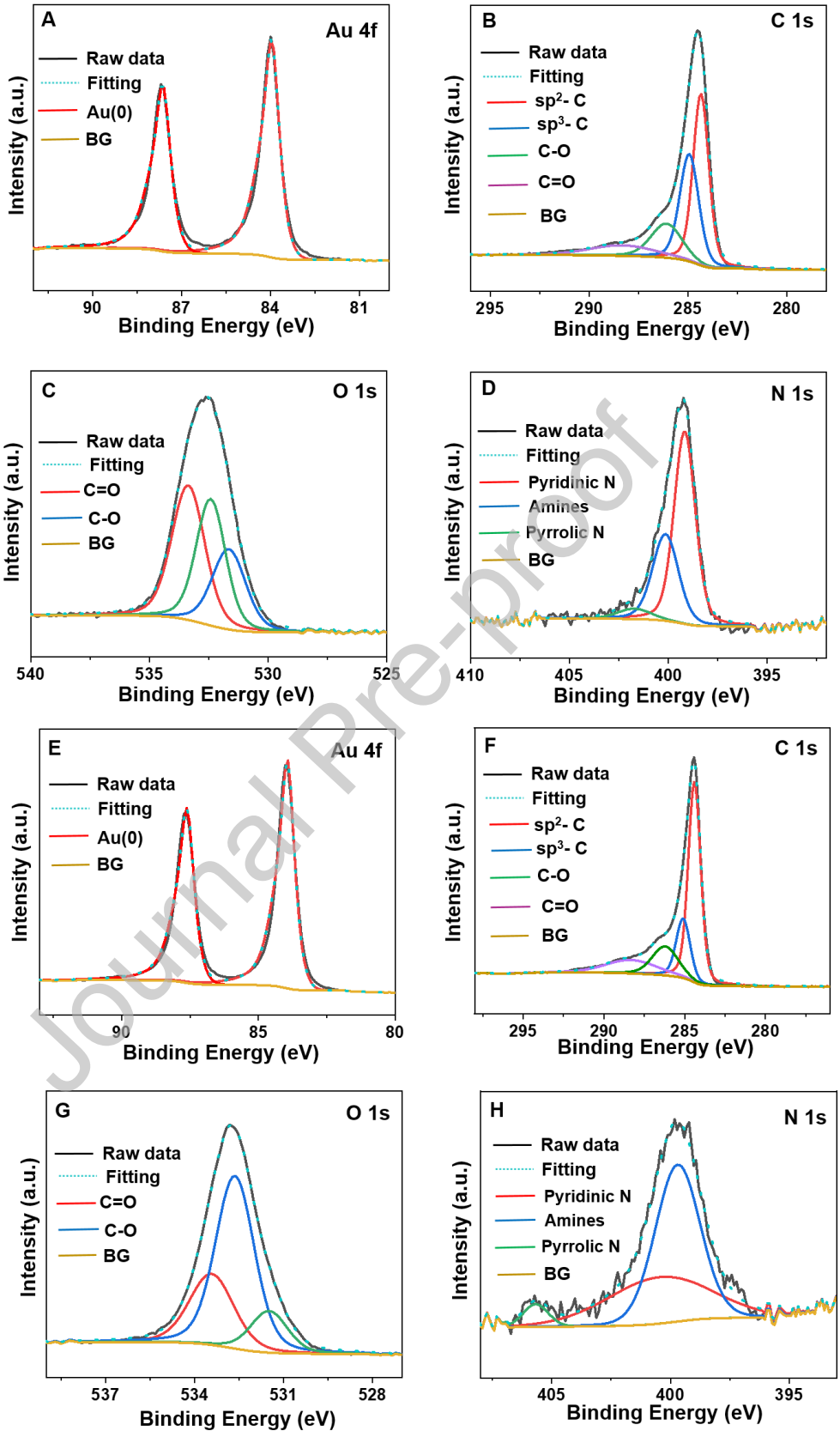

Figure 3. XPS deconvoluted spectra of EC-AuNP/LSGE: Au 4f (A), C 1s (B), O 1s (C), and N 1s (D). XPS deconvoluted spectra of SP-AuNP/LSGE: Au 4f (E), C 1s (F), O 1s (G), and N 1s (H).

The chemical composition of the electrodes was also studied by X-ray photoelectron spectroscopy. The deconvoluted XPS data of plain LSGE is given in **Figure S4**, presenting the expected peaks of C 1s, N 1s, and O 1s. The C 1s binding energies, 284.2, 284.8, 285.9 and 288.0 eV can be assigned to C-C (sp^2 C), sp^3 C, C-O, and C=O, respectively. The peak corresponding to the sp^2 carbon is the most prominent one, because most of the carbon present in the LSGE is graphitized. The deconvoluted N 1s peak originates from the residual nitrogen doping because of the use of a nitrogen environment during laser treatment. Indeed, it is interesting to note that nitrogen doping within graphene sheets can be done concomitantly with graphene formation, through laser irradiation. The O 1s peak shows typical bands for surface oxygen functionalities, which are consistent with the previous reports [2, 34]. **Figure 3** displays the deconvoluted XPS peaks of EC-AuNP/LSGE and SP-AuNP/LSGE. Both EC-AuNP/LSGE and SP-AuNP/LSGE are featured with Au 4f, C 1s, N 1s, and O 1s peaks. The C 1s and Au 4f bands of EC-AuNP/LSGE and SP-AuNP/LSGE are presented peaks for C-C, C-O, C=O, and Au (0) bonds. The C 1s and Au 4f spectra of both EC-AuNP/LSGE and SP-AuNP/LSGE are very similar, differing only in intensity. This similarity suggests that the chemical nature of the materials in both EC-Au and SP-Au is the same. The deconvoluted N 1s shows pyridinic N, amines, and pyrrolic N for both EC-AuNP/LSGE and SP-AuNP/LSGE. However, the ratio of amines and pyrrolic N are significantly varied. Excessive amines over pyrrolic N are observed for EC-AuNP/LSGE, whereas the opposite trend is observed for SP-AuNP/LSGE. Most likely, this is because of the differences in the nucleation sites at the electrodeposition and sparking methods, which requires further investigations. The deconvoluted O 1s spectra of EC-AuNP/LSGE and SP-AuNP/LSGE show no significant differences [34] .

Next XRD and Raman data of the plain LSGE, EC-AuNP/LSGE, and SP-AuNP/LSGE are analyzed. The XRD patterns of SP-AuNP/LSGE feature a graphitic crystal pattern evident from the peak at 26.3° corresponding to the crystal structures of the (002) plane (**Figure 4**A). In addition, signature patterns of AuNPs were observed at 38.2°, 44.3°, 64.7°, 77.7°, and 81.7° corresponding to the planes of (111), (200), (220), (311), and (222) respectively.[37] The XRD results indicate that both electrodeposition and spark-discharge methods are quite effective in providing crystalline Au NPs. Raman data of the SP-AuNPs, EC-AuNPs, and plain LSGE are analyzed (**Figure 4**B). A characteristic Raman pattern was observed for SP-AuNP/LSGE, containing D, G, and 2D bands located at 1340.5 cm^{-1}, 1569.4 cm^{-1}, and 2673.9 cm^{-1}, respectively. This pattern is consistent with the expected Raman patterns for graphene structures.[34, 38] The Raman bands of EC-AuNPs and plain LSGE have also shown D, G, and 2D bands at similar locations. However, the intensity of the bands varied slightly among these three materials. Especially, the D/G band ratio gives some crucial information regarding defects. The D/G band

ratio of SP-AuNP/LSGE, EC-AuNP/LSGE, and plain LSGE are calculated to be, 0.78, 0.92, and 0.75, respectively. The D/G band ratio of SP-AuNP/LSGE and plain LSGE are similar, suggesting that the graphene sheet structure is perceived and not affected by the sparking discharge process. On the other hand, the D/G band ratio of EC-AuNP/LSGE is increased by 22.67% compared with the plain LSGE. The use of HCl in the electrochemical synthesis of AuNPs largely affects the sheet structure which is also evident from the morphology studies discussed in the previous sections. Interestingly, the D/G band ratio of SP-AuNP/LSGE is increased by just 4% when compared with the plain LSGE, indicating that the graphene sheets were not adversely affected by the spark-discharge process.

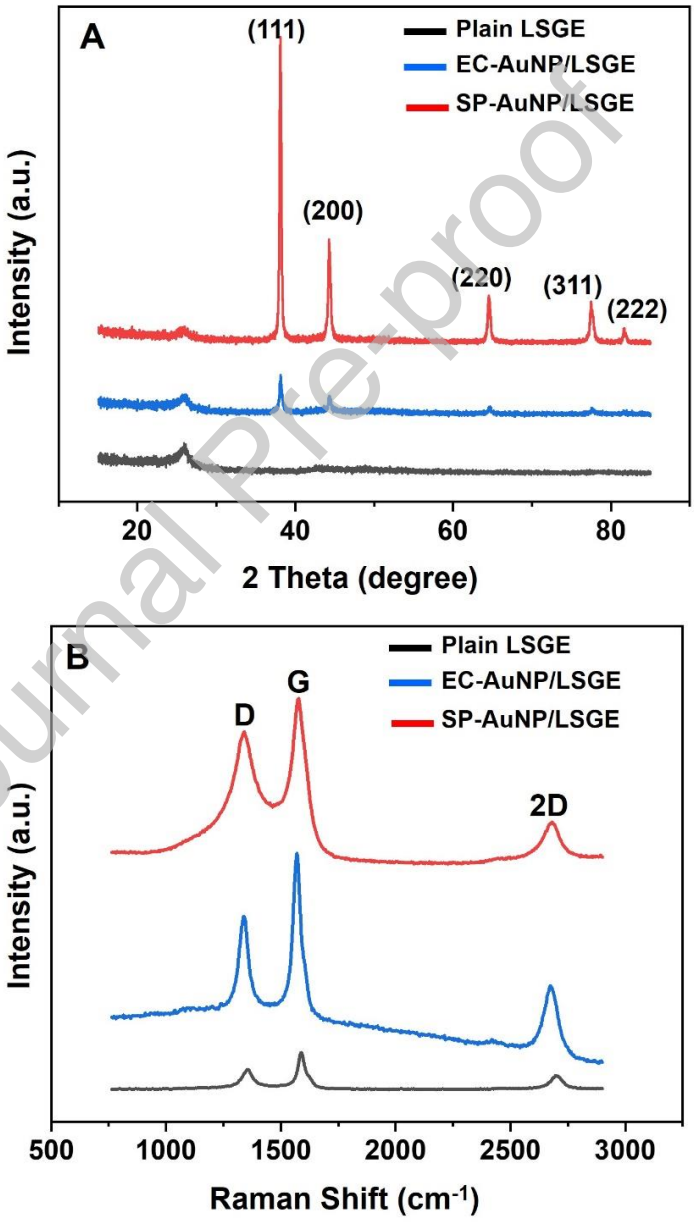

Figure 4. (A) XRD and (B) Raman patterns of plain LSGE (black), EC-AuNP/LSGE (blue), and SP-AuNP/LSGE (red).

Next, Kelvin probe force microscopy (KPFM) analysis was employed to investigate potential differences in the surface potentials of SP-AuNP/LSGE and EC-AuNP/LSGE. The electronic work functions of SP-AuNP/LSGE and EC-AuNP/LSGE, denoted as ϕSP and ϕEC, respectively, were compared using KPFM. This technique allows the determination of the contact potential difference (CPD), providing insights into charge carrier concentration. The CPD values obtained were utilized to calculate the work function (ϕ) of the samples using Equation (1):

$$\text{CPD (V)} = \phi_{TIP} - \phi_{SAMPLE} \qquad \text{(eq. 1)}$$

Here, ϕ_{TIP} is the work function of the KPFM tip, and ϕ_{SAMPLE} is the work function of the sample. Our methodology involved first establishing ϕ_{TIP} using a Bruker SCM-PIT-V2 tip, coated with PtIr. For this, we employed a highly ordered pyrolytic graphite (HOPG) standard, with a known work function of 4.6 eV, to calibrate our system. The CPD value from HOPG **(Figure S5)**, measured at 231.1 mV, in conjunction with its known work function (4.6 eV), enabled us to determine ϕ_{TIP} as 4.8 eV using Equation (1).

To obtain CPD_{EC}, we have performed KPFM mapping of the EC-AuNP/LSGE sample under test (**Figure 5A**). The surface and KPFM mapping of the EC-AuNP/LSGE sample under test can be seen in **Figures 5B** and **5C**, respectively. We calculated the work function of EC-AuNP/LSGE sample (ϕ_{EC}) using Equation (2):

$$\phi_{EC} = \phi_{TIP} - CPD_{EC} \qquad \text{(eq. 2)}$$

The CPD_{EC} value, derived from KPFM mapping, was −380.8 mV, leading to a ϕ_{EC} of approximately 5.2 eV.

The setup employed to do KPFM analysis of the SP-AuNP/LSGE sample under test is shown in **Figure 6D**. The surface and KPFM mapping of the sample under test can be seen in **Figures 6E and 6F**. For the SP-AuNP/LSGE sample, we used Equation (3) to determine its work function (ϕ_{SP}):

$$\phi_{SP} = \phi_{TIP} - CPD_{SP} \qquad \text{(eq. 3)}$$

The CPD_{SP} was measured as −113.9 mV, yielding a ϕ_{SP} of approximately 4.9 eV.

Consequently, we observed that ϕ_{EC} and ϕ_{SP} values are 5.2 eV and 4.9 eV, respectively. The lower work function of the SP-AuNP/LSGE sample, compared with that of the EC-AuNP/LSGE, by

about 0.27 eV, is likely due to a higher electron availability (**Figures 5G** and **5H**). This difference suggests a potential for greater oxidation and reduction currents in the SP-AuNP/LSGE sample relative to the EC-AuNP/LSGE sample.

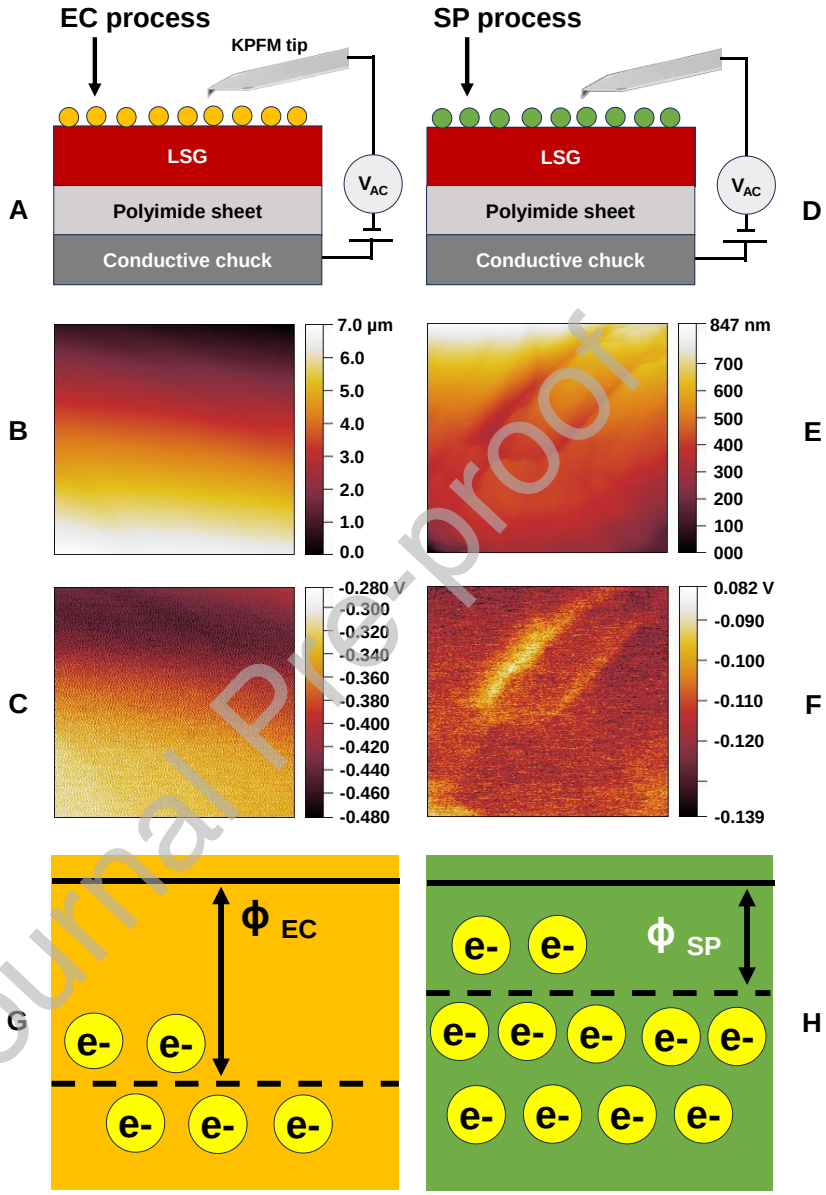

Figure 5. KPFM setup and analysis data for EC-AuNP/LSGE (A-C, G) and SP-AuNP/LSGE (D-F, H).

3.2. Electrochemical properties

Figure 6A shows the cyclic voltammograms of the EC-AuNP/LSGE, SP-AuNP/LSGE, and plain LSGE in 0.1 M H_2SO_4. All the electrodes showed a reduction peak around − 0.120 V, which is due to the

reduction reaction of dissolved oxygen. Other than the oxygen reduction peak, plain LSGE showed no significant peaks. Whereas both SP-AuNP/LSGE and EC-AuNP/LSGE showed additional peaks that are expected to originate from the AuNPs. In the forward anodic run, SP-AuNP/LSGE shows a peak around 0.90 V attributed to the reduction of AuO, but this peak is not clearly observed in the voltammogram of EC-AuNP/LSGE. Generally, the characteristic Au oxidation peak appears as a shoulder peak when AuNPs are associated with graphene support, such reports are ubiquitous among graphene/AuNP-based literature reports [37]. During the reverse cathodic run, a prominent peak was observed at + 0.36 V for both EC-AuNP/LSGE, SP-AuNP/LSGE, which can be correlated to the reduction of the gold oxide layer (insets to **Figure 6**A). Both the anodic and cathodic peak currents at SP-AuNP/LSGEare relatively larger compared with EC-AuNP/LSGE.

Next, the electrochemical behavior of the electrodes has been tested in potassium ferri/ferro cyanide model system (**Figure 6**B and **Figure S6**). The anodic peak current (I_{pa}), cathodic peak currents (I_{pc}), and peak-to-peak separation values (ΔE_p) are estimated. The I_{pa}, I_{pc}, and ΔE_p at the SP-AuNP/LSGE are 124.78 µA, -136.67 µA, and 160 mV. The I_{pa}, I_{pc}, and ΔE_p at the EC-AuNP/LSGE are 106.96 µA, -120.25 µA, and 153 mV, respectively. Both SP-AuNP/LSGE and EC-AuNP/LSGE have shown increased peak currents compared with plain LSGE indicating a significant increase in the surface area because of AuNPs. The difference between the ΔEp of the EC-AuNPs and SP-Au NPs is only around 7 mV, which is not a significant value. On the other hand, SP-AuNP/LSGE exhibit much higher peak currents—both cathodic and anodic—than EC-AuNP/LSGE, and slightly improved I_{pa}/I_{pc} ratio of 0.91 compared with 0.89 in EC-AuNP/LSGE indicating that the former exhibit overall a better electrochemical reversibility and redox behavior.

Next, the EIS Nyquist plots of the EC-AuNP/LSGE, SP-AuNP/LSGE, and plain LSGE are assessed (**Figure 6**C). The interfacial charge-transfer resistance (R_{ct}) values are estimated to be 130.5 **Ω**, 50.4 **Ω**, and 14.7 **Ω** for plain LSGE, EC-Au NPs/LSGE, and SP-Au NPs/LSGE, respectively. Because of the high conductivity of AuNPs, a considerable drop in R_{ct} was seen when EC-AuNPs or SP-AuNPs were placed on the LSGE surface, while in comparison to EC-AuNPs, SP-AuNPs displayed a significantly lower R_{ct}. Based on the various physicochemical and electrochemical characterization studies, the following conclusions can be drawn: (1) the particle size of the spark generated AuNPs is smaller compared with the that of the electroplated AuNPs. This fact results in an increased Au loading and accessibility in SP-AuNP/LSGE, (2) The surface-to-volume ratio of SP-AuNPs is significantly higher than that of EC-AuNPs, (3), The sheet-like structure of the graphene is perceived in SP-AuNPs but damaged in EC-AuNPs, which likely affects the edge densities of the graphene sheets in EC-AuNP/LSGE.

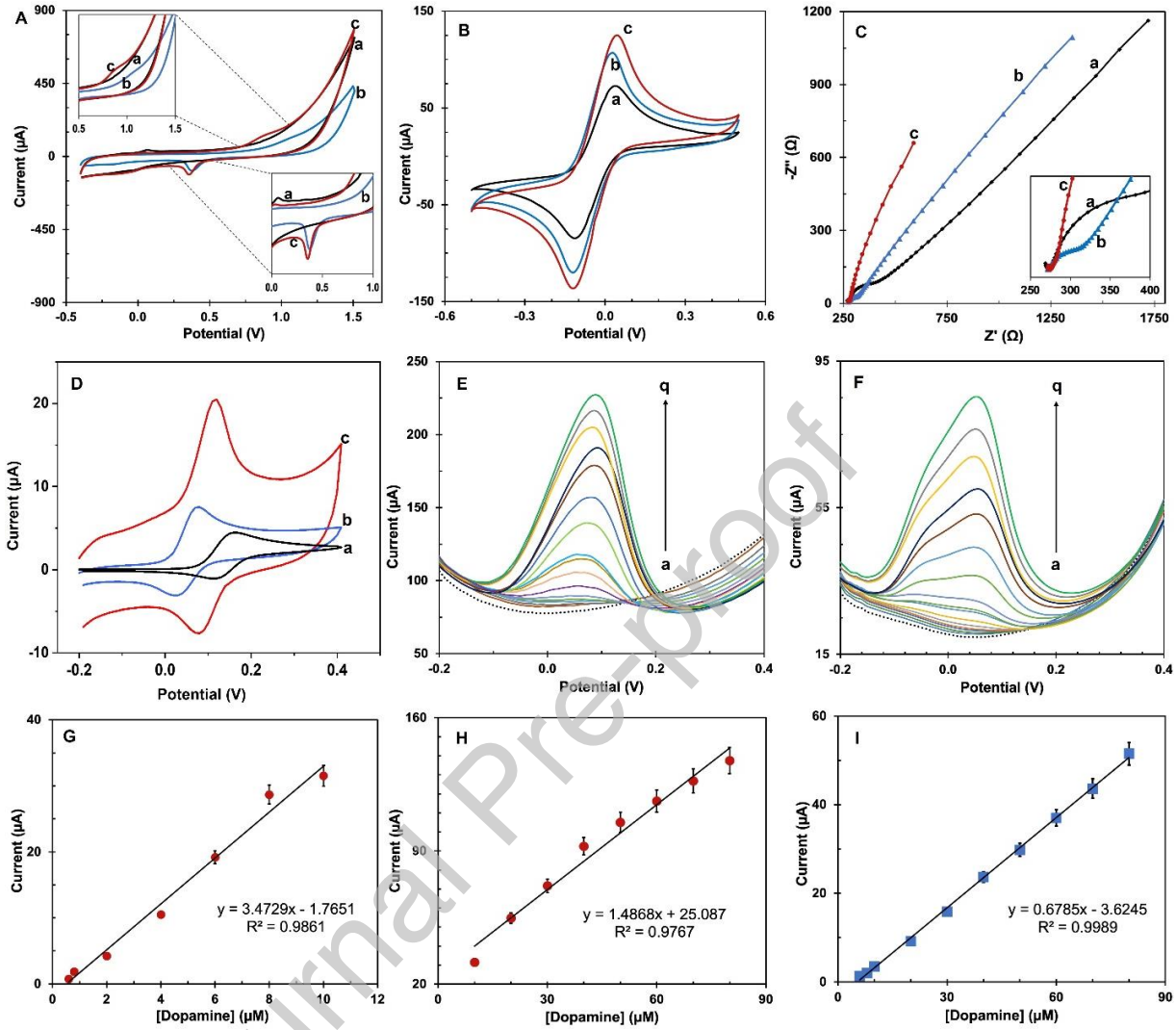

Figure 6. CV characteristics of (a) plain LSGE, (b) EC-AuNP/LSGE, and (c) SP-AuNP/LSGE at 100 mV/s, in **(A)** 0.10 M H_2SO_4, and **(B)** 5.0 mM $K_3[Fe(CN)_6]/K_4[Fe(CN)_6]$ in 0.1 M PBS; scan rate: 100 mV/s. **(C)** EIS spectra of SP-AuNP/LSGE, EC-AuNP/LSGE, and plain LSGE in 0.1 M PBS, pH 7 containing 5+5 mM $K_3[Fe(CN)_6]/K_4[Fe(CN)_6]$. Insets show enlarged views of the peaks. SP-AuNP/LSGE, EC-AuNP/LSGE, and plain LSGE are shown in red, blue, and black color lines respectively. **(D)** Dopamine analysis: CVs of SP-AuNP/LSGE (red), EC-AuNP/LSGE (blue), and unmodified LSGE (black) towards 20 μM dopamine. DPV responses of SP-AuNP/LSGE **(E)** and EC-AuNP/LSGE **(F)** to different concentrations of dopamine: a=0, b=0.2, c=0.4, d=0.6, e=0.8, f=2.0, g=4.0, h=6.0, i=8.0, j=10, k=20, l=30, m=40, n=50, o=60, p=70, and q=80 μM dopamine. Calibration plots for

dopamine with SP-AuNP/LSG; linear range 1 **(G)** and linear range 2 **(H)**. Calibration plots for dopamine with EC-AuNP/LSGE **(I).**

3.3. Electrochemical sensing properties

Dopamine was used as a model analyte to examine the electrochemical sensing capabilities of the SP-AuNP/LSGE, EC-AuNP/LSGE, and plain LSGE. Previous works have demonstrated that graphene and AuNPs composites are extremely selective for dopamine [37]. The CV responses of the electrodes to dopamine are given in **Figure 6D**. All the electrodes presented a well-defined redox signals, which can be correlated to the dopamine oxidation reaction [39, 40]. As evident from the redox signal data, SP-AuNP/LSGE and EC-AuNP/LSGE outperform unmodified LSGE, which is clearly ascribed to the excellent electrochemical properties of AuNPs. Next, the electrochemical data among SP-AuNPs and EC-AuNPs are closely analyzed. The I_{pa}, I_{pc}, ΔE_p, formal potential ($E^{o'}$) are 20.45 µA, -7.66 µA, 40 mV, and 0.099 V respectively for SP-AuNP/LSGE. The I_{pa}, I_{pc}, ΔE_p, and $E^{o'}$ are 7.53 µA, -3.11 µA, 60 mV, and 0.0497 respectively for EC-AuNP/LSGE. The I_{pa}, I_{pc}, ΔE_p, and $E^{o'}$ are 4.47 µA, -1.08 µA, 50 mV, and 0.135 V respectively for plain LSGE. The I_{pa} of dopamine at SP-AuNPs showed at least 2.7-fold enhanced peak current compared to EC-AuNPs indicating a faster electron transport kinetics at the SP-AuNPs compared to EC-AuNPs. In addition, the ΔE_p value indicate a slightly faster electron transport kinetics at SP-AuNPs compared to EC-AuNPs. The formal potential value of the SP-AuNPs is slightly decreased compared to plain LSGE. The dopamine electroanalysis investigation suggests that the Au nanoparticles generated by sparking discharge provided an excellent signal amplification for developing dopamine sensors.

Next, different concentrations of dopamine were measured with SP-AuNP/LSGE and EC-AuNP/LSGE to further examine their sensing capacities (**Figure 6**E, F). The current signals of both SP-AuNPs and EC-AuNPs rise linearly with an increase in dopamine concentration. For the same tested dopamine levels, the response signals using SP-AuNPs are at least two times higher compared to EC-AuNPs. Another observation is that the SP-AuNPs can measure dopamine at concentration up to 0.8 µM, whereas the EC-AuNPs are unable to detect dopamine levels below 4.0 µM. Thus, the sensing capacity of the electrode can be greatly enhanced by switching from electrodeposition to spark-discharge AuNPs production. A linear regression plots shown in **Figure 8**G-I, was created using DPV data. The EC-AuNP showed a linear range of 6.0–80 µM and a detection limit of 4.0 µM. The SP-AuNP displayed two linear ranges (0.6-10 µM and 10-80 µM), and a detection limit of 0.40 µM. Interestingly, about 10-fold enhanced detection limit is achieved by SP-AuNP compared to EC-AuNP. The dopamine detection sensitivity was 0.678 µA/µM at EC-AuNP/LSGE. The sensitivity was 3.473 µA/µM for the first linear range and 1.487 µA/µM for the second linear range. About 5.12 (first range) and 2.2 (second range) folds

increased signal sensitivities are observed when SP-AuNPs are used for dopamine. Thus, SP-AuNPs are showing better dopamine sensing ability compared to EC-AuNPs. The excellent signal amplification property, greater number of Au loading, increased Au accessibility, increased surface-to-volume ratio, and undamaged graphene sheet structure are the probable reasons why SP-AuNPs outperform EC-AuNPs.

The electroanalytical parameters are compared with previously reported works in **Table 1**. The SP-AuNP/LSGE showed comparable performance with existing reports. It is worth to mention that most of the graphene reports presented in the table are made from conventional chemically synthesized graphene. The conventional chemical synthesis is solution-based, laborious, time-consuming, necessitates huge amounts of harsh chemicals, and encounters aggregation issues [41]. In contrast, the production of LSGE is easy, fast, reagent-free, and aggregation-free, additionally LSGEs are disposable, flexible, and performs better than conventional electrodes such as glassy carbon electrodes [22, 42]. Moreover, the sparking method and procedures for AuNPs productions are easy to be automatized for roll-to-roll manufacturing and therefore ideal for large scale manufacturing.

Table 1. Electrochemical sensing performance of SP-AuNP/LSGE with previously reported works.

Electrodes	Technique	pH	Linear Range (μM)	LOD (μM)	Validation
Graphene quantum dots@MWCNTs/ /GCE [43]	DPV	PBS (pH 7.0)	0.25-250	0.095	Human serum
Carbon quantum dots/CuO/GCE [44]	SWV	PBS (pH 7.0)	1-180	25.4	Dopamine hydrochloride injection
Electrochemically reduced graphene oxide/GCE [45]	DPV	PBS (pH 7.0)	0.5-60	0.5	Human urine
Co_3O_4 nanocubes/MWCNTs/GCE [46]	CA	PBS (pH 7.2)	1-20	0.176	Urine sample
MnO_2/MWCNTs/electrochemically treated GCE [47]	DPV	PBS (pH 7.0)	1.0-50	0.8	Human serum
PA6/PAH-MWCNTs/ITO [48]	DPV	PBS (pH 7.0)	1-70	0.15	-
Cylindrical Au nanoelectrodes/ITO [49]	CV	PBS (pH 7.4)	1-100	5.83	Human neuroblastoma cells (SH-SY5Y)
Spark-discharge produced AuNPs/LSGE (this work)	DPV	PBS (pH 7.4)	0.6–90	0.40	Human neuroblastoma cells (SH SY5Y),

human serum

*Abbreviations: MWCNTs: Multiwalled carbon nanotubes; GCE: Glassy carbon electrodes; EPGCE: Electrochemically pretreated glassy carbon electrodes; PA6/PAH-MWCNTs: polyamide 6/poly(allylamine hydrochloride) nanofibers functionalized with multiwalled carbon nanotubes; ITO: Indium tin oxide electrode; DPV: Differential pulse voltammetry; SWV: Square wave voltammetry; CA: Chronoamperometry; CV: Cyclic voltammetry.

3.4. Selectivity, reproducibility, stability, and practicality

The selectivity of the sensor towards dopamine detection was investigated in the presence of common interfering agents such as glucose, uric acid, and ascorbic acid. The DPV results are given in **Figure S7A-C** and presented as a bar chart in **Figure 7**A. When tested alone with SP-AuNP/LSGE sensor, glucose showed negligible signal, ascorbic acid showed less than 3% signal, and uric acid showed about 6% signal. Although ascorbic acid and uric acid showed notable DPV signals, but their detection potentials are away from dopamine signal, i.e., about 0.0 V for ascorbic acid, and 0.30 V for uric acid. The current values are measured at potential where dopamine showed its maximum DPV signal. In addition, additional tests are conducted to check whether the co-existence of these interfering compounds can induce any measurable interferences to the dopamine signal. As shown in the red bars of **Figure 7A**, the dopamine signal was slightly oscillated when the interferences are co-existed, however, the level of interference was still less than 7.5%. The dopamine selectivity of the electrode can be explained based on electrostatic interactions. The electrode contains a negatively charged surface because of graphene which inhibits negatively charged interfering compounds such as ascorbic acid.

The reproducibility of the sensor is tested with five different SP-AuNP/LSGE sensors (**Figure S8**). Relative standard deviations (R.S.D) of 5.53% were observed for the tested electrodes, suggesting appreciable reproducibility (**Figure 7B**). This indicates that the spark discharge method is robust in producing reproducible electrodes. The stability of the SP-AuNP/LSGE was investigating its voltammetric signal to ferricyanide system before and after six months. **Figure S9** shows the CV curves of stability test, while **Figure 7C** presents the bar chart plotted with the anodic peak currents (I_{pa}) and cathodic peak currents (I_{pc}). About 89.8% (I_{pa}) and 78.3% (I_{pc}) have been retained after six months of its storage, suggesting outstanding storage stability of the electrode. The electrode was stored at ambient conditions without any special storage conditions. In the CV data of the electrode stored for six months, the formal potential of the redox couple shifted slightly to the anodic side. This shift could be attributed to the use of laser-graphene as the reference and counter electrodes. To avoid this, a stable reference electrode, such as Ag/AgCl, could be used. However, we chose this way to simplify the electrode fabrication process.

The stability results along with reproducibility results indicate the AuNPs are strongly adhered to the graphene sheets and the material is highly stable and retains its electrochemical properties [50]. There are several possible interactions between graphene and AuNPs that provide the stability, which are extensively studied in the literature elsewhere. A notable interaction is the electrostatic attraction between the positively charged AuNPs and negatively charged regions (e.g., defects, functional groups) on graphene.

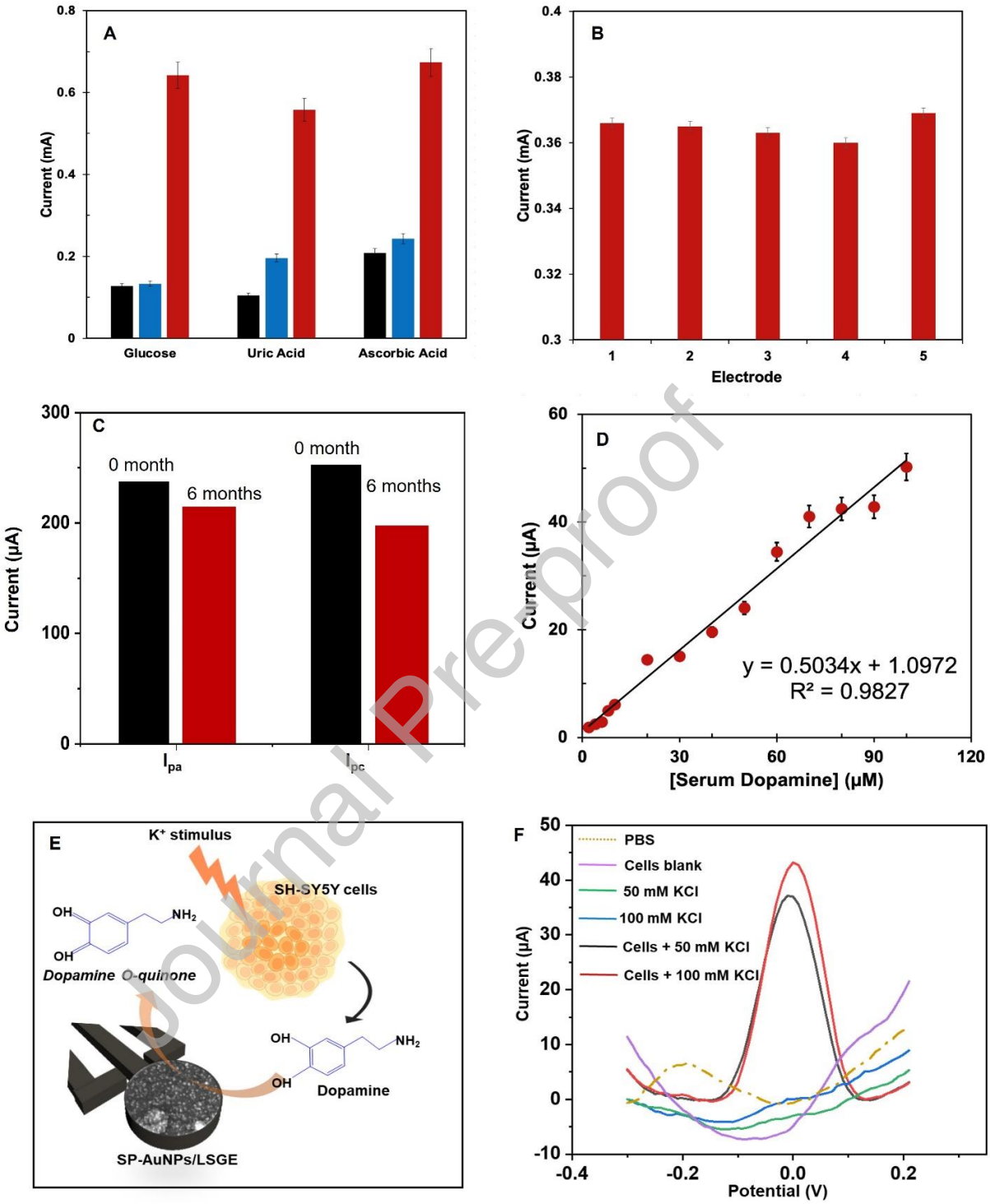

Figure 7. (A) Selectivity of SP-AuNP/LSGE to 2.0 mM dopamine with respect to 2.0 mM glucose, 2.0 mM uric acid, and 2.0 mM ascorbic acid. Here, black bar, blue bar, and red bar represent control, 2.0 mM respective interfering compounds, and 2.0 mM respective interfering compounds+2.0 mM dopamine. **(B)** Reproducibility of five SP-AuNP/LSGE. DPVs were recorded for 1.0 mM dopamine and the current

signal was used to plot the bar chart. **(C)** stability test. Bar chart for anodic (I_{pa}) and cathodic (I_{pc}) peak currents of ferricyanide solution before (black bar) and after six months storage (red bar) of SP-AuNP/LSGE. **(D)** Calibration plot for dopamine spiked human serum analysis using SP-AuNP/LSGE. **(E)** A schematic scheme for stimulant induced *in-situ* dopamine productions from SH-SY5Y cells and concomitant detections with SP-AuNP/LSGE sensor. **(F)** DPVs of SH-SY5Y cells stimulated with 50 mM and 100 mM KCl and control experiments (cells + no stimulant, no cells + stimulant).

The practical feasibility of the SP-AuNP/LSGE was tested in a human serum sample. The serum sample was found dopamine-free. To imitate real-world conditions, dopamine in the range of 1.0 µM to 100 µM was spiked into the serum samples. Then, SP-AuNP/LSGE was used to test the dopamine-spiked samples. As shown in **Figure S10**, the sensor displayed distinct DPV response signals to each concentration of dopamine-spiked serum samples, ranging from 15 µM to 100 µM. A linear regression plot is prepared from DPV curves, and the corresponding equation is, I (µA) = 0.5034 [Dopamine] (µM) + 1.097 (**Figure 7D)**. The linear range is slightly different from the linear range obtained for the same analysis performed in PBS. The likely reason is that the human serum provides a more complex solution background that includes a variety of proteins and biomolecules. Because of their ensemble presence, the detection range at the lower end of the linear range is not that much great. The sensor can still detect up to 1.0 µM level of dopamine, but those data points are not making the linear range.

3.5 Monitoring in-situ dopamine synthesis in neuroblastoma cell line

The determination of *in-situ* dopamine is essential to comprehend the pharmacology, physiology, and pathology of dopamine associated diseases. The practical feasibility of the SP-AuNP/LSGE sensor was tested for monitoring dopamine released from live cells. The SH SY5Y cell line of neuroblastoma cells was used as a model for producing in-situ dopamine [51]. The K^+ stimulation was applied to induce the cells to produce dopamine, which was detected [49, 52]. DPV experiments were performed with SH SY5Y live cells with and without KCl stimulations. The generation of in-situ dopamine with stimulation is schematically depicted in **Figure 7E** and the corresponding DPV results are presented in **Figure 7F**. These neuroblastoma cells were cultured and then stimulated with two different concentration 50 mM and 100 mM of KCl which forcefully induces stress on to the cells making then release dopamine, after waiting for 30 mins DPV spectra were collected. The solution containing only cells showed no significant peaks, followed by the solution containing KCl (50 mM and 100 mM), which also had no notable peaks. On the other hand, the cells stimulated with KCl indicated a deterministic peak at 37.12 µA and 43.18 µA for 50 mM and 100 mM respectively. However, the current changes obtained from the cells were

correlated to the calibration curve and the concentration of the dopamine releases was indicated to be 16.71 μM and 20.05 μM which agrees with the previous reports [32, 53]. The results also indicates that the cells have reached a saturation point at which they are no longer able to produce more dopamine, which explains why the dopamine measurements did not double despite the stimulant's concentration being doubled. Based on the cell studies, we can conclude that it is possible to quantitatively detect dopamine using SP-AuNP sensor.

4. Conclusions

In summary, we developed a novel, eco-friendly solid-state synthesis method for producing gold nanoparticles on laser-scribed graphene electrodes, surpassing traditional electrochemical synthesis in preserving graphene integrity and generating uniformly distributed, ultrathin nanoparticles. Our findings reveal that AuNPs produced via the spark-discharge method exhibit superior electrochemical sensing capabilities, including a 10-fold improvement in the detection for dopamine, compared to those prepared through electrodeposition. Furthermore, the application of SP-AuNPs/LSGE in the in-situ detection of dopamine production from neuroblastoma cells not only demonstrates the method's practical applicability but also its potential to significantly advance the field of electrochemical sensing. The promising results obtained from the spark discharge method open new avenues for the synthesis of AuNPs and potentially other metal nanoparticles and bimetallic alloys on LSG electrodes, setting a new benchmark for the development of highly sensitive and efficient electrochemical sensors. The spark-discharge technique represents a significant advance in electrochemical sensor development, offering a promising new approach for high-sensitivity biosensing applications.

Acknowledgments

The authors would like to express their acknowledgments to the financial support of funding from King Abdullah University of Science and Technology (KAUST), Saudi Arabia. The authors also thank Prof. Jan Hrbac (Masaryk University, Brno, CZ) for providing the HV power supply.

References

[1] A.A. Lahcen, S. Rauf, T. Beduk, C. Durmus, A. Aljedaibi, S. Timur, H.N. Alshareef, A. Amine, O.S. Wolfbeis, K.N. Salama, Electrochemical sensors and biosensors using laser-derived graphene: A comprehensive review, Biosensors and Bioelectronics, 168 (2020) 112565.

[2] T. Beduk, D. Beduk, J.I. de Oliveira Filho, F. Zihnioglu, C. Cicek, R. Sertoz, B. Arda, T. Goksel, K. Turhan, K.N. Salama, Rapid point-of-care COVID-19 diagnosis with a gold-nanoarchitecture-assisted laser-scribed graphene biosensor, Analytical chemistry, 93 (2021) 8585-8594.

[3] H. Wang, Y. Sun, X. Liu, T. Li, CO_2 laser-induced formation of a nitrogen-doped graphene aerophobic layer on the nickel foam surface for enhanced electro-oxidation of urea, Surfaces and Interfaces, 46 (2024) 104074.

[4] Y. Lei, A.H. Alshareef, W. Zhao, S. Inal, Laser-scribed graphene electrodes derived from lignin for biochemical sensing, ACS Applied Nano Materials, 3 (2019) 1166-1174.

[5] F.M. Vivaldi, A. Dallinger, A. Bonini, N. Poma, L. Sembranti, D. Biagini, P. Salvo, F. Greco, F. Di Francesco, Three-dimensional (3D) laser-induced graphene: structure, properties, and application to chemical sensing, ACS Applied Materials & Interfaces, 13 (2021) 30245-30260.

[6] L.F. Mendes, A. de Siervo, W. Reis de Araujo, T.R. Longo Cesar Paixão, Reagentless fabrication of a porous graphene-like electrochemical device from phenolic paper using laser-scribing, Carbon, 159 (2020) 110-118.

[7] S. Rauf, V. Mani, A.A. Lahcen, S. Yuvaraja, T. Beduk, K.N. Salama, Binary transition metal oxide modified laser-scribed graphene electrochemical aptasensor for the accurate and sensitive screening of acute myocardial infarction, Electrochimica Acta, 386 (2021) 138489.

[8] Z. You, Q. Qiu, H. Chen, Y. Feng, X. Wang, Y. Wang, Y. Ying, Laser-induced noble metal nanoparticle-graphene composites enabled flexible biosensor for pathogen detection, Biosensors and Bioelectronics, 150 (2020) 111896.

[9] A. Berni, A.A. Lahcen, A. Amine, Electrochemical sensing of paracetamol using 3D porous laser scribed graphene platform, Electroanalysis, 35 (2023) e202200137.

[10] B. Purohit, A. Kumar, R. Kumari, K. Mahato, S. Roy, A. Srivastava, P. Chandra, 3D gold dendrite and reduced graphene oxide-chitosan nanocomposite-based immunosensor for carcinoembryonic antigen detection in clinical settings, Surfaces and Interfaces, 47 (2024) 104197.

[11] P. Arul, S.-T. Huang, V. Mani, C.-H. Huang, Gold–Silver Bimetallic Alloy Nanoparticles in a Covalent Organic Framework for Real-Time Monitoring of Hydrogen Peroxide from Live Cells, ACS Applied Nano Materials, 5 (2022) 6340-6351.

[12] S.A. Bansal, V. Kumar, J. Karimi, A.P. Singh, S. Kumar, Role of gold nanoparticles in advanced biomedical applications, Nanoscale Advances, 2 (2020) 3764-3787.

[13] L. Qin, G. Zeng, C. Lai, D. Huang, P. Xu, C. Zhang, M. Cheng, X. Liu, S. Liu, B. Li, "Gold rush" in modern science: fabrication strategies and typical advanced applications of gold nanoparticles in sensing, Coordination Chemistry Reviews, 359 (2018) 1-31.
[14] A. Ghanam, A.A. Lahcen, T. Beduk, H.N. Alshareef, A. Amine, K.N. Salama, Laser scribed graphene: A novel platform for highly sensitive detection of electroactive biomolecules, Biosensors and Bioelectronics, 168 (2020) 112509.
[15] B. Zhu, L. Yu, S. Beikzadeh, S. Zhang, P. Zhang, L. Wang, J. Travas-Sejdic, Disposable and portable gold nanoparticles modified - laser-scribed graphene sensing strips for electrochemical, non-enzymatic detection of glucose, Electrochimica Acta, 378 (2021) 138132.
[16] A. Scroccarello, R. Álvarez-Diduk, F. Della Pelle, C. de Carvalho Castro e Silva, A. Idili, C. Parolo, D. Compagnone, A. Merkoçi, One-Step Laser Nanostructuration of Reduced Graphene Oxide Films Embedding Metal Nanoparticles for Sensing Applications, ACS Sensors, 8 (2023) 598-609.
[17] T. Beduk, M. Gomes, J.I. De Oliveira Filho, S.S. Shetty, W. Khushaim, R. Garcia-Ramirez, C. Durmus, A. Ait Lahcen, K.N. Salama, A portable molecularly imprinted sensor for on-site and wireless environmental bisphenol A monitoring, Frontiers in chemistry, 10 (2022) 833899.
[18] J. Liu, B. Zhu, H. Dong, Y. Zhang, M. Xu, J. Travas-Sejdic, Z. Chang, A novel electrochemical insulin aptasensor: From glassy carbon electrodes to disposable, single-use laser-scribed graphene electrodes, Bioelectrochemistry, 143 (2022) 107995.
[19] G. Wang, J. Chen, L. Huang, Y. Chen, Y. Li, A laser-induced graphene electrochemical immunosensor for label-free CEA monitoring in serum, Analyst, 146 (2021) 6631-6642.
[20] A.A. Lahcen, S. Rauf, A. Aljedaibi, J.I. de Oliveira Filho, T. Beduk, V. Mani, H.N. Alshareef, K.N. Salama, Laser-scribed graphene sensor based on gold nanostructures and molecularly imprinted polymers: Application for Her-2 cancer biomarker detection, Sensors and Actuators B: Chemical, 347 (2021) 130556.
[21] W. Khushaim, K. Peramaiah, T. Beduk, M.T. Vijjapu, J.I. de Oliveira Filho, K.-W. Huang, V. Mani, K.N. Salama, Porous graphitic carbon nitrides integrated biosensor for sensitive detection of cardiac troponin I, Biosensors and Bioelectronics: X, 12 (2022) 100234.
[22] S. Rauf, A.A. Lahcen, A. Aljedaibi, T. Beduk, J.I. de Oliveira Filho, K.N. Salama, Gold nanostructured laser-scribed graphene: A new electrochemical biosensing platform for potential point-of-care testing of disease biomarkers, Biosensors and Bioelectronics, 180 (2021) 113116.
[23] I. Saldan, O. Dobrovetska, L. Sus, O. Makota, O. Pereviznyk, O. Kuntyi, O. Reshetnyak, Electrochemical synthesis and properties of gold nanomaterials, Journal of Solid State Electrochemistry, 22 (2018) 637-656.

[24] A.V. Papavasileiou, T. Hoder, T. Medek, M.I. Prodromidis, J. Hrbac, Sensitive riboflavin sensing using silver nanoparticles deposited onto screen-printed electrodes via controlled-energy spark discharges, Talanta, 258 (2023) 124409.
[25] D. Riman, K. Spyrou, A.E. Karantzalis, J. Hrbac, M.I. Prodromidis, Glucose sensing on graphite screen-printed electrode modified by sparking of copper nickel alloys, Talanta, 165 (2017) 466-473.
[26] P.-A. Kolozof, A.B. Florou, K. Spyrou, J. Hrbac, M.I. Prodromidis, In-situ tailoring of the electrocatalytic properties of screen-printed graphite electrodes with sparked generated molybdenum nanoparticles for the simultaneous voltammetric determination of sunset yellow and tartrazine, Sensors and Actuators B: Chemical, 304 (2020) 127268.
[27] M.G. Trachioti, A.E. Karantzalis, J. Hrbac, M.I. Prodromidis, Low-cost screen-printed sensors on-demand: Instantly prepared sparked gold nanoparticles from eutectic Au/Si alloy for the determination of arsenic at the sub-ppb level, Sensors and Actuators B: Chemical, 281 (2019) 273-280.
[28] N.S. Tabrizi, M. Ullmann, V.A. Vons, U. Lafont, A. Schmidt-Ott, Generation of nanoparticles by spark discharge, Journal of Nanoparticle Research, 11 (2009) 315-332.
[29] A. Kohut, L. Ludvigsson, B.O. Meuller, K. Deppert, M.E. Messing, G. Galbács, Z. Geretovszky, From plasma to nanoparticles: optical and particle emission of a spark discharge generator, Nanotechnology, 28 (2017) 475603.
[30] M.G. Trachioti, E.I. Tzianni, D. Riman, J. Jurmanova, M.I. Prodromidis, J. Hrbac, Extended coverage of screen-printed graphite electrodes by spark discharge produced gold nanoparticles with a 3D positioning device. Assessment of sparking voltage-time characteristics to develop sensors with advanced electrocatalytic properties, Electrochimica Acta, 304 (2019) 292-300.
[31] Q. Huang, X. Lin, L. Tong, Q.-X. Tong, Graphene Quantum Dots/Multiwalled Carbon Nanotubes Composite-Based Electrochemical Sensor for Detecting Dopamine Release from Living Cells, ACS Sustainable Chemistry & Engineering, 8 (2020) 1644-1650.
[32] X. Zan, H. Bai, C. Wang, F. Zhao, H. Duan, Graphene Paper Decorated with a 2D Array of Dendritic Platinum Nanoparticles for Ultrasensitive Electrochemical Detection of Dopamine Secreted by Live Cells, Chemistry – A European Journal, 22 (2016) 5204-5210.
[33] A. Kovtun, D. Jones, S. Dell'Elce, E. Treossi, A. Liscio, V. Palermo, Accurate chemical analysis of oxygenated graphene-based materials using X-ray photoelectron spectroscopy, Carbon, 143 (2019) 268-275.
[34] T. Beduk, J.I. de Oliveira Filho, A. Ait Lahcen, V. Mani, K.N. Salama, Inherent Surface activation of laser-scribed graphene decorated with au and ag nanoparticles: Simultaneous electrochemical behavior toward uric acid and dopamine, Langmuir, 37 (2021) 13890-13902.

[35] X. Liu, Y. Han, J.W. Evans, A.K. Engstfeld, R.J. Behm, M.C. Tringides, M. Hupalo, H.-Q. Lin, L. Huang, K.-M. Ho, D. Appy, P.A. Thiel, C.-Z. Wang, Growth morphology and properties of metals on graphene, Progress in Surface Science, 90 (2015) 397-443.
[36] P. Nayak, N. Kurra, C. Xia, H.N. Alshareef, Highly Efficient Laser Scribed Graphene Electrodes for On-Chip Electrochemical Sensing Applications, Advanced Electronic Materials, 2 (2016) 1600185.
[37] V.K. Ponnusamy, V. Mani, S.-M. Chen, W.-T. Huang, J.-F. Jen, Rapid microwave assisted synthesis of graphene nanosheets/polyethyleneimine/gold nanoparticle composite and its application to the selective electrochemical determination of dopamine, Talanta, 120 (2014) 148-157.
[38] T. Beduk, A.A. Lahcen, N. Tashkandi, K.N. Salama, One-step electrosynthesized molecularly imprinted polymer on laser scribed graphene bisphenol a sensor, Sensors and Actuators B: Chemical, 314 (2020) 128026.
[39] S.S. Shetty, J.K. El-Demellawi, Y. Khan, M.N. Hedhili, P. Arul, V. Mani, H.N. Alshareef, K.N. Salama, Iron Single-Atom Catalysts on MXenes for Ultrasensitive Monitoring of Adrenal Tumor Markers and Cellular Dopamine, Advanced Materials Technologies, n/a 2202069.
[40] X. Liu, J. Liu, Biosensors and sensors for dopamine detection, View, 2 (2021) 20200102.
[41] N. Kumar, R. Salehiyan, V. Chauke, O. Joseph Botlhoko, K. Setshedi, M. Scriba, M. Masukume, S. Sinha Ray, Top-down synthesis of graphene: A comprehensive review, FlatChem, 27 (2021) 100224.
[42] R. Ye, D.K. James, J.M. Tour, Laser-induced graphene: from discovery to translation, Advanced Materials, 31 (2019) 1803621.
[43] S.K. Arumugasamy, S. Govindaraju, K. Yun, Electrochemical sensor for detecting dopamine using graphene quantum dots incorporated with multiwall carbon nanotubes, Applied Surface Science, 508 (2020) 145294.
[44] S.E. Elugoke, O.E. Fayemi, A.S. Adekunle, B.B. Mamba, T.T.I. Nkambule, E.E. Ebenso, Electrochemical sensor for the detection of dopamine using carbon quantum dots/copper oxide nanocomposite modified electrode, FlatChem, 33 (2022) 100372.
[45] L. Yang, D. Liu, J. Huang, T. You, Simultaneous determination of dopamine, ascorbic acid and uric acid at electrochemically reduced graphene oxide modified electrode, Sensors and Actuators B: Chemical, 193 (2014) 166-172.
[46] A. Numan, M.M. Shahid, F.S. Omar, S. Rafique, S. Bashir, K. Ramesh, S. Ramesh, Binary nanocomposite based on Co3O4 nanocubes and multiwalled carbon nanotubes as an ultrasensitive platform for amperometric determination of dopamine, Microchimica Acta, 184 (2017) 2739-2748.
[47] Y. Wang, L. Wang, Q. Zhuang, A ratiometric electrochemical sensor for dopamine detection based on hierarchical manganese dioxide nanoflower/multiwalled carbon nanotube nanocomposite modified glassy carbon electrode, Journal of Alloys and Compounds, 802 (2019) 326-334.

[48] L.A. Mercante, A. Pavinatto, L.E.O. Iwaki, V.P. Scagion, V. Zucolotto, O.N. Oliveira, Jr., L.H.C. Mattoso, D.S. Correa, Electrospun Polyamide 6/Poly(allylamine hydrochloride) Nanofibers Functionalized with Carbon Nanotubes for Electrochemical Detection of Dopamine, ACS Applied Materials & Interfaces, 7 (2015) 4784-4790.

[49] D.-S. Kim, E.-S. Kang, S. Baek, S.-S. Choo, Y.-H. Chung, D. Lee, J. Min, T.-H. Kim, Electrochemical detection of dopamine using periodic cylindrical gold nanoelectrode arrays, Scientific Reports, 8 (2018) 14049.

[50] D. Hernández-Sánchez, G. Villabona-Leal, I. Saucedo-Orozco, V. Bracamonte, E. Pérez, C. Bittencourt, M. Quintana, Stable graphene oxide–gold nanoparticle platforms for biosensing applications, Physical Chemistry Chemical Physics, 20 (2018) 1685-1692.

[51] H. Xicoy, B. Wieringa, G.J.M. Martens, The SH-SY5Y cell line in Parkinson's disease research: a systematic review, Molecular Neurodegeneration, 12 (2017) 10.

[52] M. Senel, M. Dervisevic, S. Alhassen, A. Alachkar, N.H. Voelcker, Electrochemical Micropyramid Array-Based Sensor for In Situ Monitoring of Dopamine Released from Neuroblastoma Cells, Analytical Chemistry, 92 (2020) 7746-7753.

[53] B.-X. Shi, Y. Wang, K. Zhang, T.-L. Lam, H.L.-W. Chan, Monitoring of dopamine release in single cell using ultrasensitive ITO microsensors modified with carbon nanotubes, Biosensors and Bioelectronics, 26 (2011) 2917-2921.

Author Statement

Saptami Suresh Shetty: Writing – review & editing, Methodology, Investigation, Formal analysis, Validation,

Lavita Nuraviana Rizalputri: Methodology, Investigation, Formal analysis,

Maria G. Trachioti: Methodology, Investigation, Formal analysis,

Saravanan Yuvaraja: Methodology, Validation,

Veerappan Mani: Writing – original draft; Writing – review & editing, Formal analysis, Conceptualization, Validation,

Mamas I. Prodromidis: Writing – review & editing, Formal analysis, Conceptualization, Supervision, Funding acquisition, Validation, Investigation

Khaled Nabil Salama: Writing – review & editing, Formal analysis, Conceptualization, Supervision, Funding acquisition, Investigation,

Declaration of interests

☒ The authors declare that they have no known competing financial interests or personal relationships that could have appeared to influence the work reported in this paper.

☐The authors declare the following financial interests/personal relationships which may be considered as potential competing interests:

Graphical Abstract